Electronic Supplementary Material (ESI) for Nanoscale.

BSA-caged metal clusters to exfoliate MoS_2 nanosheets towards their hybridized functionalization

Guijian Guan,*[a] Shuhua Liu,[a] Yuan Cheng,[b] Yong-Wei Zhang,*[b] and Ming-Yong Han*[a]

[a] Institute of Materials Research and Engineering, A*STAR, 2 Fusionopolis Way, Singapore 138634

E-mail: guan_guijian@imre.a-star.edu.sg

my-han@imre.a-star.edu.sg

[b]Institute of High Performance Computing, A*STAR, 1 Fusionopolis Way, Singapore 138632

E-mail: zhangyw@ihpc.a-star.edu.sg

Calculation Method.

Binding energies of different species with Ag^+ ions Ag atom. The plane wave code Vienna *ab initio* simulation package (VASP) was used to simulate the binding energies of different species with Ag^+ ions and Ag atom within the framework of density functional theory (DFT). First, the individual energy of species or compounds was calculated via the conformation optimization by using projector augmented wave method with the PW91 functional. Then, the binding energies were determined by calculating the difference between the energy of compound and the energy of individual species in total.

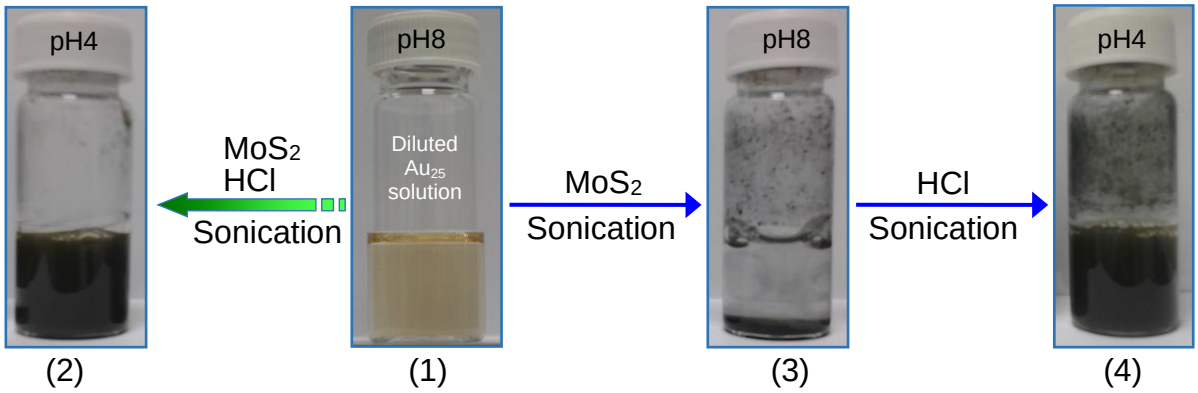

Fig. S1 pH-dependent exfoliation of MoS_2 nanosheets in the solution of BSA-caged Au_{25} clusters. After diluting 2 mL of as-purified Au_{25} clusters in PBS solution with distilled water by 5 times (**1**), the resulting pH8 solution was adjusted to pH4 with 1M HCl followed by introducing 50 mg of MoS_2 powder and sonicating for 48 h to produce Au_m/MoS_2 nanosheets (**2**). For comparison, the direct addition of MoS_2 powder into the as-diluted Au_{25} solution at pH8 did not lead to effective exfoliation of MoS_2 powder upon sonication for 48 h (**3**). The further adjustment of pH from 8 to 4, the exfoliation of MoS_2 nanosheets occurred upon sonication for 48 h (**4**).

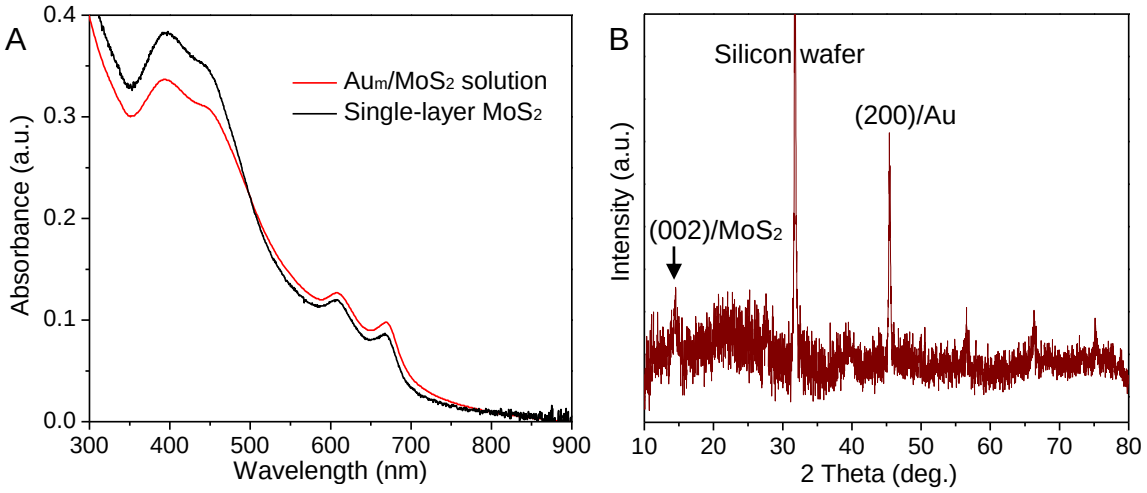

Fig. S2 Characterization of Au_m/MoS_2 nanosheets: (A) UV-vis absorption spectra and (B) XRD pattern. The ultrathin thickness of MoS_2 layers in Au_m/MoS_2 nanosheets is revealed by their similar absorption peaks to that of single-layer MoS_2 together with the weak intensity in XRD peak of MoS_2 nanosheets at ~15°. The presence of Au_m NPs is revealed by XRD peak at ~46° resulted from Au (200). Due to the epitaxial growth of Au_m NPs on MoS_2 nanosheets interfaced via (111) planes, the XRD peak from Au (111) is not observed.

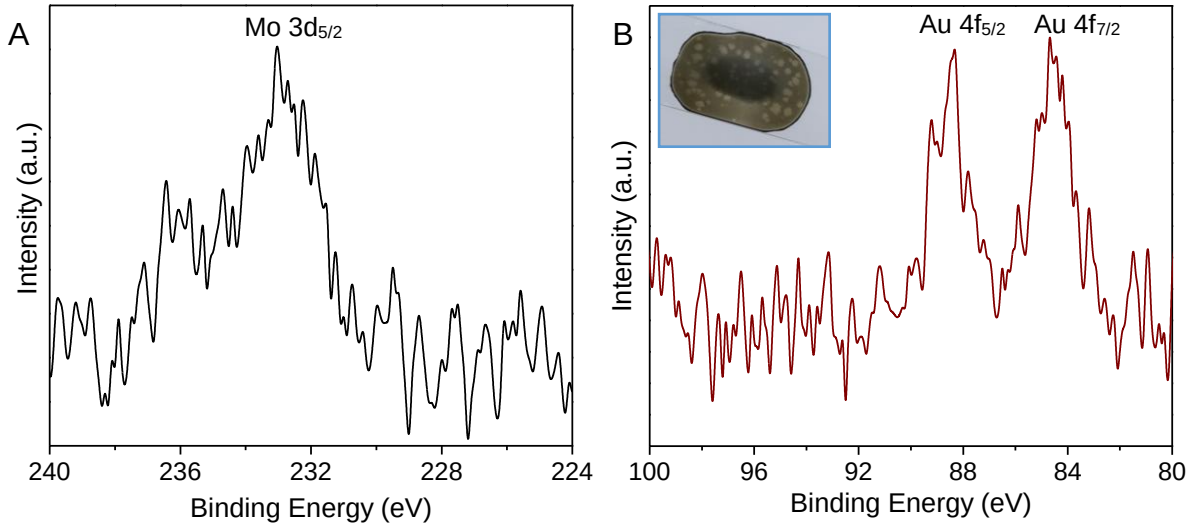

Fig. S3 X-ray photoelectron spectroscopy (XPS) spectra of Au_m/MoS_2 nanosheets for analyzing the elements of (A) Mo and (B) Au. The XPS sample was prepared by dropping and drying Au_m/MoS_2 nanosheets on glass substrate, as shown in the inset optical image in (B).

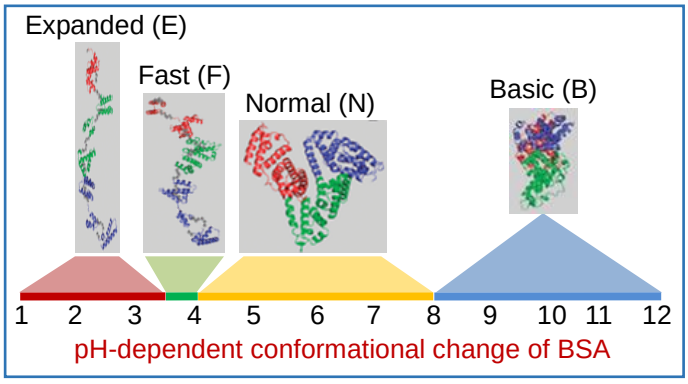

Fig. S4 Conformations of BSA at different pH values. BSA has a typical conformation with the "heart" shape at pH 4.3–8.0 while expanding to adopt a faster migrating form at 4.3–3.5, and further stretched at pH < 3.5. At pH > 8.0, BSA takes a basic conformation with loss of rigidity.

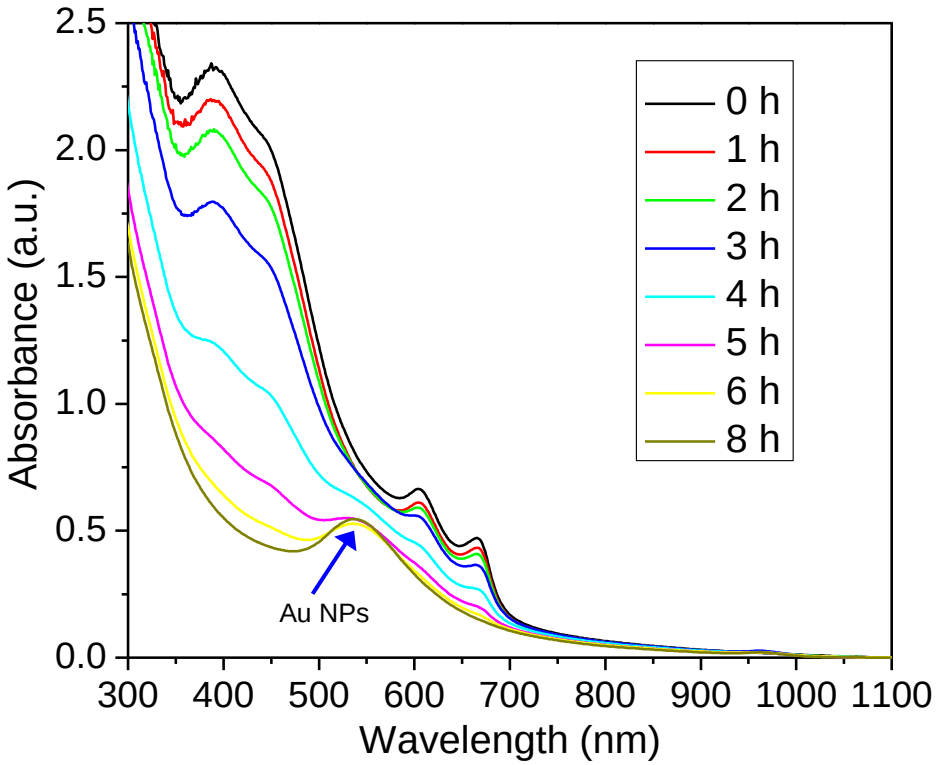

Fig. S5 UV-vis absorption spectral evolution from Au_m/MoS_2, Au_{m+n}/MoS_2 nanosheets to 50 nm Au NPs after adding 50 mM H_2O_2 into Au_m/MoS_2 solution. The absorption peaks of MoS_2 nanosheets at 400, 605 and 666 nm gradually decrease with the increase of incubation time until disappear at 8 h. Meanwhile, a new absorption peak is observed at 540 nm to indicate the formation of Au NPs.

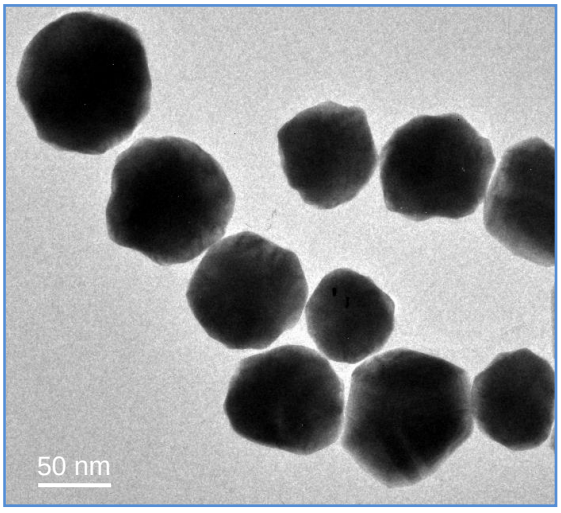

Fig. S6 TEM image of Au NPs obtained after adding H_2O_2 to 50 mM in the solution of Au_m/MoS_2 nanosheets and incubating for 8 h.

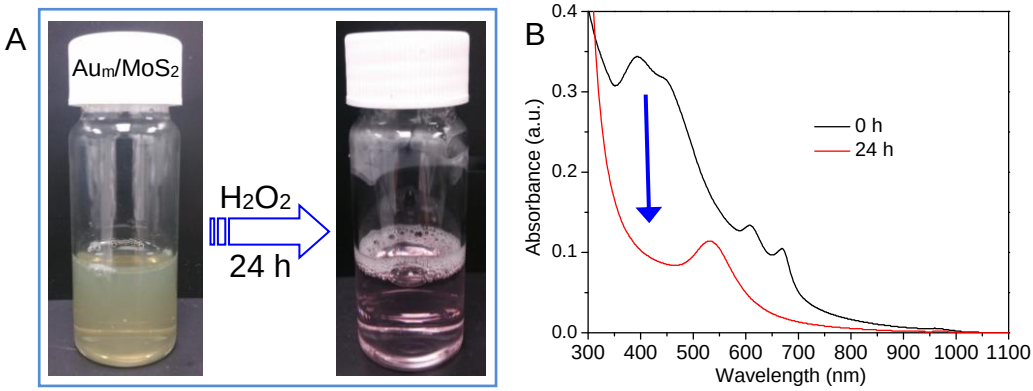

Fig. S7 Optical and spectral change of Au_m/MoS_2 nanosheets in pH4 solution upon the addition of 50 mM H_2O_2 for 24 h. (A) Optical images and (B) UV-vis absorption spectra of Au_m/MoS_2 solution after reaction with H_2O_2 for 24 h. The color change from greenish brown to magenta and corresponding evolution of absorption spectra indicate that the further growth of Au NPs occurred upon the introduction of H_2O_2 accompanied by the dissolution of MoS_2 nanosheets.

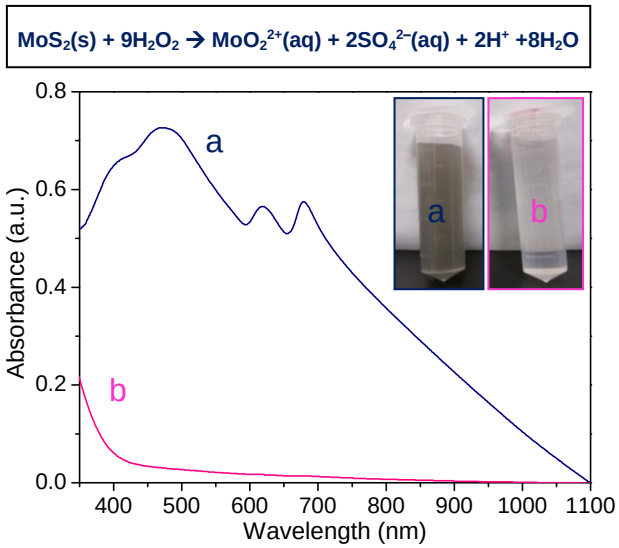

Fig. S8 UV-vis absorption spectra and optical images (inset) of MoS_2 in pH4 solution before (a) and after treatment by 50 mM H_2O_2 for 24 h (b). The absorption peaks of MoS_2 disappeared accompanied with the color change from brown to colorless, indicating the chemical dissolution of MoS_2 in H_2O_2 solution.

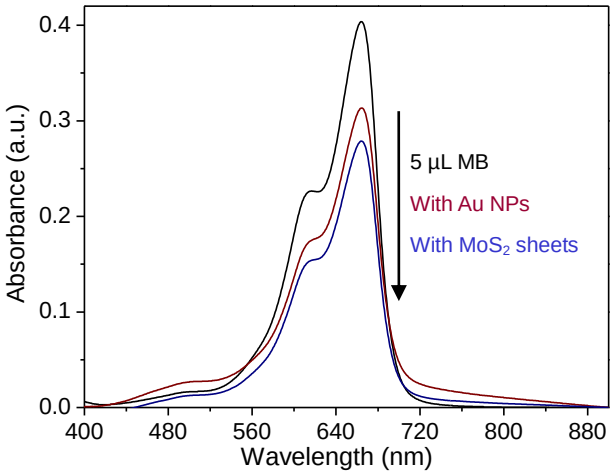

Fig. S9 Photocatalytic degradation of methylene blue (MB) by Au NPs or MoS_2 nanosheets. The black line is the UV-vis absorption spectrum of 5 µM MB solution. The red and blue lines are the UV-vis absorption spectra of 5 µM MB solution after photocatalytic degradation by Au NPs and MoS_2 nanosheets, respectively. Experimentally, the photocatalytic degradation of MB was performed under a solar simulator for 40 min, and then the resulting solutions were centrifuged at 10000 rpm to remove Au NPs or MoS_2 nanosheets before collecting the spectra of supernatants. According to the change of absorption intensity, the percentages of photocatalytic degradation are calculated to be 22.5% and 30% for Au NPs and MoS_2 nanosheets, respectively.

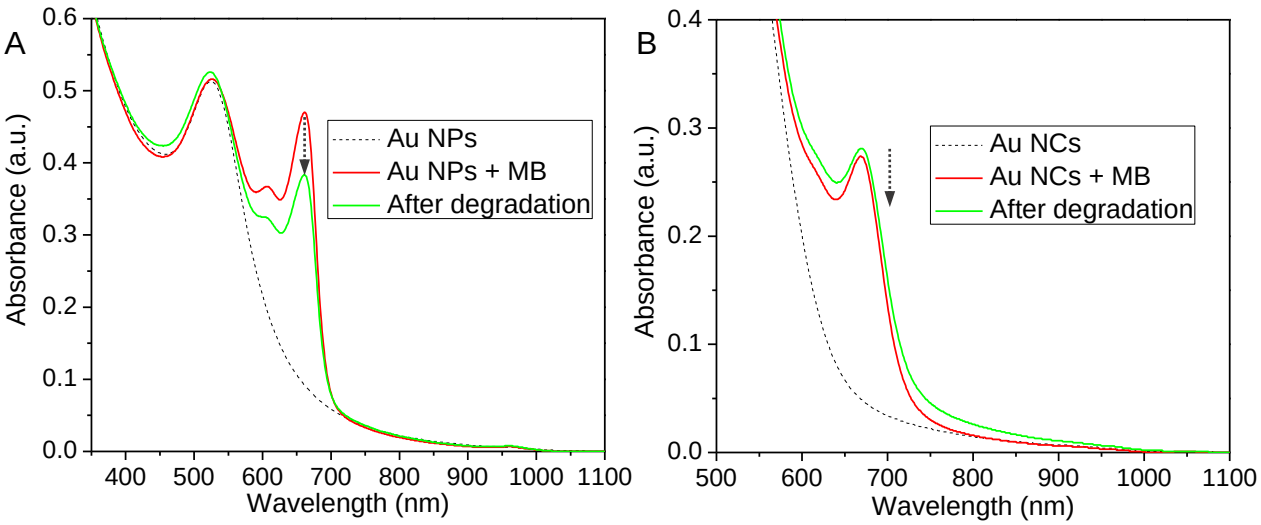

Fig. S10 Photocatalytic degradation of MB in the solutions of Au NPs (A) and Au_{25} nanoclusters (Au NCs) (B). Experimentally, an aqueous solution of 5 µM MB in the presence of Au NPs or NCs was stirred for 10 min, and then left under a solar simulator for 40 min before collecting their absorption spectra. Based on the change of absorption intensity, the percentages of photocatalytic degradation were calculated to be 19.5% and 3.5% for Au NPs and Au NCs, respectively. As compared to the measurement of supernatant after removal of Au NPs, the in-situ measured result has a smaller value due to the scattering of Au NPs.

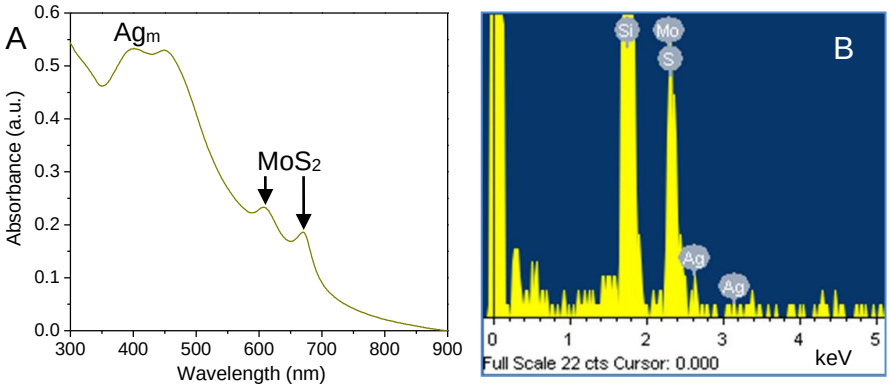

Fig. S11 Experimental evidences for the production of Ag_m/MoS_2 nanosheets: (A) UV-vis absorption spectrum, and (B) EDX image on silicon substrate.

Table. S1 The calculated energies of individual species and their complex pairs for revealing the growth mechanism of Ag NPs from Ag nanoclusters, which were calculated by using the first-principle software VASP with the PW91 functional.

Species	Ag^0	Ag^+	$–SR^–$	$OH^–$	RSSR
Energy (eV)	-1025.70	-1019.84	-482.55	-452.84	-961.70

Pairs	$Ag^0–Ag^0$	$Ag^0–Ag^+$	$Ag^+–SR^–$	$Ag^+–OH^–$	Ag^+–RSSR
Energy (eV)	-2053.99	-2047.99	-1507.77	-1477.85	-1985.03
Binding Energy (eV)	2.59	2.45	5.38	5.17	3.49

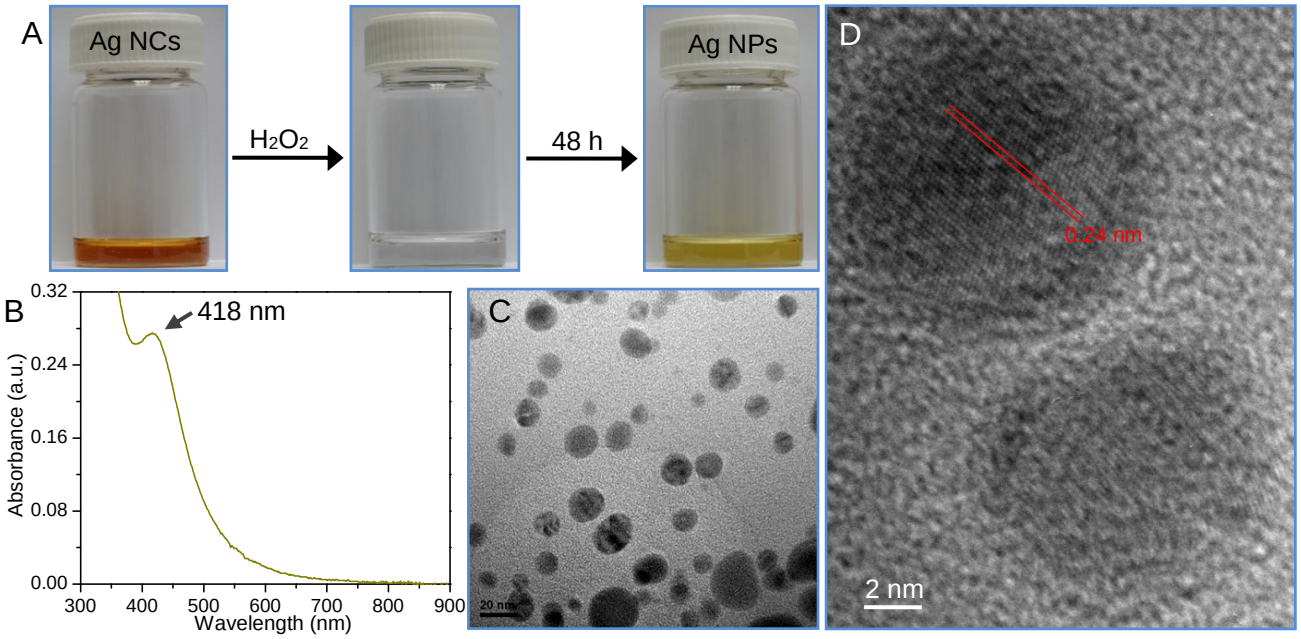

Fig. S12 Production of Ag NPs in the basic solution of BSA-caged Ag NCs upon treating with 50 mM H_2O_2. (A) Optical observation for the growth process. (B) UV-vis absorption spectrum of the Ag NPs with a plasmonic peak at 418 nm. (C) Low-resolution and (D) high-resolution TEM images of Ag NPs. The fringe spacing of 0.24 nm is indexed to (111) reflection of face-centered cubic silver.

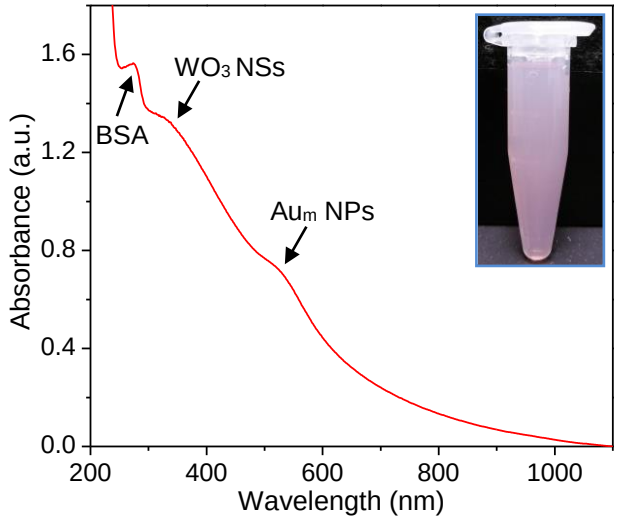

Fig. S13 UV-vis absorption spectrum and optical image (inset) of the solution containing Au_m/WO_3 nanosheets, which was obtained by sonicating 10 mL of pH4 solution containing 50 mg of WO_3 powder, 50 mM H_2O_2 and 2 mL of as-purified Au_{25} NCs in PBS solution.

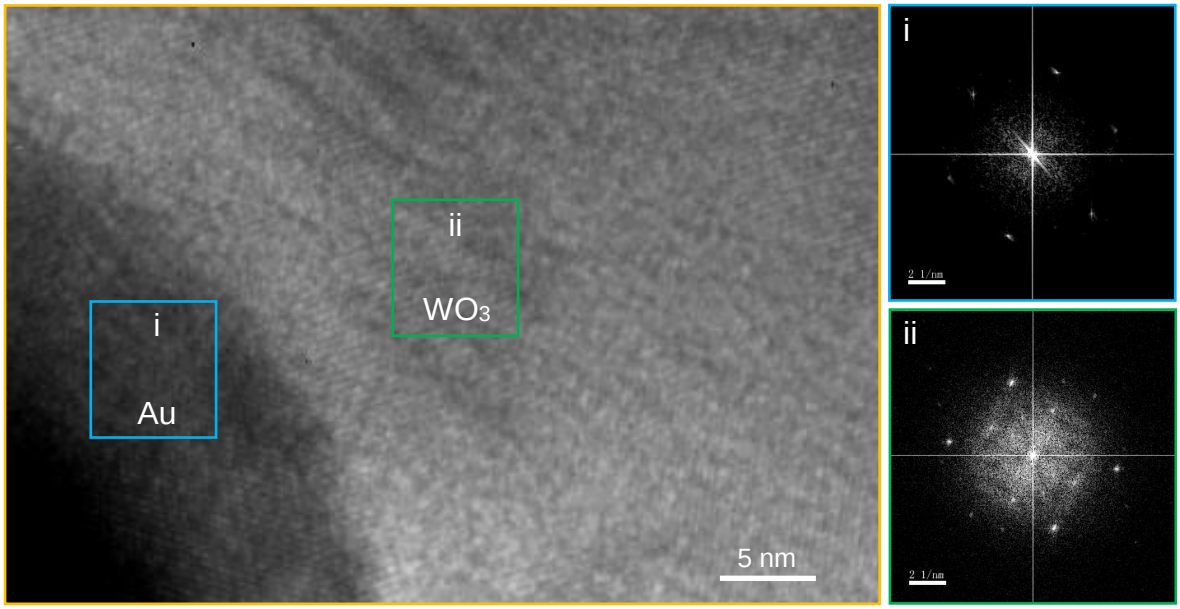

Fig. S14 Fast Fourier transform patterns in the selected regions as indicated in high-resolution TEM image of Au_m/WO_3 nanosheets, which is used to confirm the hybridization of WO_3 nanosheets with Au NPs.

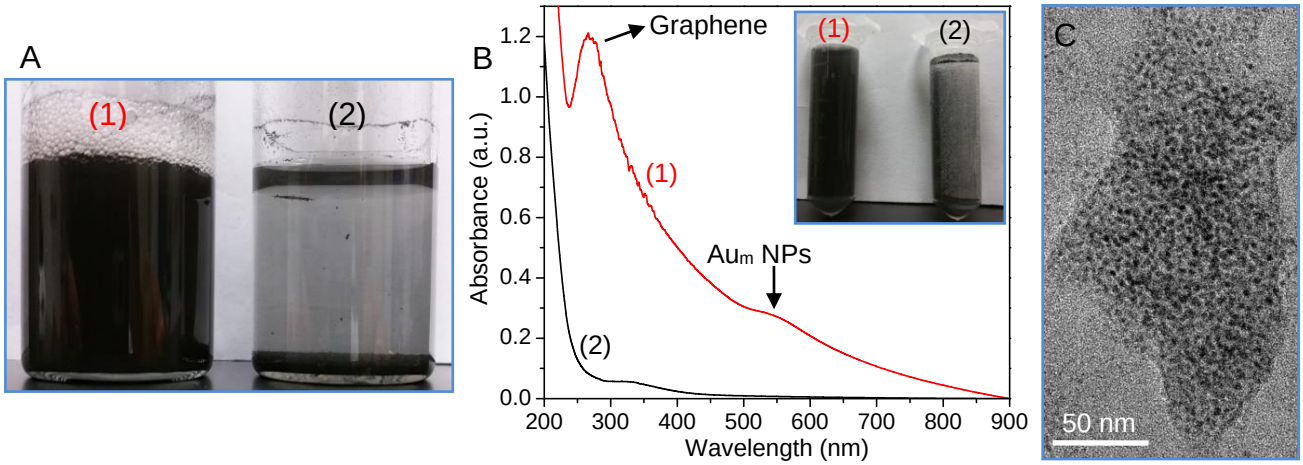

Fig. S15 Exfoliation of graphite into graphene by using BSA-caged Au_{25} clusters. (A) Optical images after sonicating graphite for 48 h in the aqueous solution of H_2O_2 in the presence (1) and absence (2) of Au_{25} clusters. The as-exfoliated solutions were first centrifuged at 4000 rpm for 20 min and then the precipitate was re-dispersed into pH4 solution via sonication. (B) UV-vis absorption spectra and optical images (inset) of the obtained solutions after further centrifugation at 1000 rpm for 10 min. (C) TEM image of Au_m/graphene nanosheets.